RC23422 (W0411-072) November 9, 2004
Materials Science

IBM Research Report

Nanoindentation Analysis of Mechanical Properties of Low to Ultra-low Dielectric Constant SiCOH Films

Lugen Wang, M. Ganor, S. I. Rokhlin
The Ohio State University
Laboratory for Multiscale Materials Processing and Characterization
Edison Joining Technology Center
1248 Arthur E. Adams Drive
Columbus, OH 43221

Alfred Grill
IBM Research Division
Thomas J. Watson Research Center
P.O. Box 218
Yorktown Heights, NY 10598

Research Division
Almaden - Austin - Beijing - Haifa - India - T. J. Watson - Tokyo - Zurich

LIMITED DISTRIBUTION NOTICE: This report has been submitted for publication outside of IBM and will probably be copyrighted if accepted for publication. It has been issued as a Research Report for early dissemination of its contents. In view of the transfer of copyright to the outside publisher, its distribution outside of IBM prior to publication should be limited to peer communications and specific requests. After outside publication, requests should be filled only by reprints or legally obtained copies of the article (e.g, payment of royalties). Copies may be requested from IBM T. J. Watson Research Center , P. O. Box 218, Yorktown Heights, NY 10598 USA (email: reports@us.ibm.com). Some reports are available on the internet at http://domino.watson.ibm.com/library/CyberDig.nsf/home.

Nanoindentation analysis of mechanical properties of low to ultra-low dielectric constant SiCOH films

Lugen Wang, M. Ganor and S. I. Rokhlin*

The Ohio State University
Laboratory for Multiscale Materials Processing and Characterization
Edison Joining Technology Center
1248 Arthur E. Adams Drive, Columbus, OH 43221

Alfred Grill

IBM-Thomas J. Watson Research Center
Yorktown Heights, New York 10598

Abstract

Carbon-doped oxide SiCOH films with low to ultralow dielectric constants have been prepared on a Si substrate by plasma-enhanced chemical vapor deposition (PECVD) from mixtures of SiCOH precursors with organic materials. The mechanical properties of the films have been characterized by continuous-stiffness nanoindentation measurements. To study the film thickness effect, each group of samples with the same dielectric constant comprised samples prepared with different film thicknesses. It is shown that the effective hardness and modulus of the film/substrate system significantly depend on indentation depth due to surface gradient plasticity and the substrate constraint effects. The "true" film properties were determined using both an empirical formulation of the effective modulus and direct inversion based on a finite element model. The hardness and modulus of three groups of samples with different degree of dielectric constants have been measured. The hardness increases from 0.7 to 2.7 GPa and modulus from 3.6 to 17.0 GPa as the dielectric constants change from 2.4 to 3.0. While for stiffer films the modulus measured at an indentation depth of 10% of film thickness is close to the "true" value for films thicker than 0.5 micron, the measured value can give an overestimate up to 35% for softer films.

I. INTRODUCTION

As the dimensions of ultralarge scale integrated (ULSI) circuits continue to shrink, optimization of the electrical properties of the interconnect dielectric becomes more important in improving the performance of ULSI devices. Such systems require materials of low dielectric constant to reduce propagation delay, cross-talk noise and power dissipation from RC coupling[1-3]. Amorphous carbon-doped glass materials (SiCOH) deposited by plasma enhanced chemical

* Corresponding author. Tel.: +1-614-292-7823; fax: +1-614-292-3395,

E-mail: rokhlin.2@osu.edu (S. I. Rokhlin)

vapor deposition (PECVD) have low to ultralow dielectric constants (*k* from 3.0 to<2.1) and are currently considered the most promising and films with dielectric constant of 3.0 are currently integrated in ULSI [3a]. The ultralow dielectric constant of SiCOH materials (k<~2.7) is achieved by introducing porosity in the films[4]. The existence of porosity significantly reduces mechanical properties such as modulus and hardness and affects the mechanical robustness of the interconnect structures incorporating such films. Therefore, for practical application of SiCOH materials in ULSI devices, it is crucial to characterize their mechanical properties such as moduli, which can be used to quantify their resistance to cracking and delamination.

Instrumented micro and nano-indentation is becoming increasingly important for measuring elasto-plastic properties on thin films [5, 7]. With very small diamond-indenter tips and high resolution of force and displacement sensing in nanoindentation instruments, the measurements are performed at the nano/micro scale. With the continuous stiffness measurement (CSM) technique[5, 7], the mechanical properties are measured continuously during the indentation test by imposing a small oscillating force during loading. This is particularly useful when testing material systems that have elastic properties varying with depth, as for example thin film systems[8-14]. Besides the mechanical properties, the fracture toughness and adhesion of thin films has been also determined using nanoindentation[12] .

Determination of the mechanical properties of soft thin films on substrates is complicated by the effects of the substrate and plasticity gradient. It is common practice to select an indentation depth less than 10% of the film thickness for “true” film properties measurement[5]. However, this selection is not applicable for very soft thin films (< 1 μm) on hard substrates because the long range elastic deformation is affected by the substrate constraint and thus the effective elastic modulus obtained by nanoindentation differs significantly from the actual modulus of the film. Several methods[10,13-15] have been proposed to determine the actual film properties from the measured effective properties for film/substrate composites. For a soft film on a substrate, another complexity in determination of film properties comes from the indentation size effect[16-18], which increases the hardness at small indentation depth.

In this study, we investigated three sets of SiCOH films of different elastic moduli and hardness and of several film thicknesses, to verify the effect of film thickness and its dependence on the film’s mechanical properties. The CSM-mode nanoindentation was applied to study the mechanical and plastic properties of the films. The “true” film properties were determined using both an empirical formulation of the effective modulus and direct inversion based on a finite element model.

II. EXPERIMENT

A. Sample preparation

SiCOH films of different dielectric constants, hence different mechanical properties, have been investigated. The films have been prepared by plasma-enhanced chemical vapor deposition (PECVD) as described in detail elsewhere[1]. Three groups of samples were prepared from different precursors using different processing conditions. Each group included several specimens prepared in identical conditions , thus with presumably similar properties, but differing film thickness. The samples are described in Table 1. The films of Group 3 are dense while those of Groups 1 and 2 are porous, Group 1 films having higher porosity [4].

B. Nanoindentation experiments

An MTS Nanoindenter® with a diamond Berkovich tip was used to characterize the SiCOH film and Si substrate. The Continuous Stiffness Measurement (CSM) indentation mode with the Dynamic Contact Module (DCM) was used to perform the measurement. Indentations were made to a prescribed depth at a constant nominal strain rate of 0.02 s^{-1}. Each result consists of an average of 12-16 indentations. Effective hardness and modulus were measured during the entire loading segment using the Oliver-Pharr method [5].

Figure 1a shows a schematic of the indentation on a film/substrate system with material sinking-in around the contact surface and Fig. 1b shows a typical loading and unloading response. Continuous stiffness indentation measurement imposes a sinusoidal force on the indenter at a frequency of about 45Hz while monitoring its displacement response, as shown in Fig. 1b. Using the measured phase and amplitude response, the dynamic contact stiffness is determined as a continuous function of indentation depth. For a homogeneous material the indentation displacement D is linearly related to the contact stiffness S (local unloading slope as shown in Fig. 1b); the indentation load P is linearly related to the square of the contact stiffness S and P is proportional to indentation depth squared (D^2) [ref. 19]:

$$P = C\ D^2\ ,\ D = C_d S\ ,\quad P = C_p S^2\ , \tag{1}$$

where C [N/m^2], C_d [m^2/N] and C_p [m^2/N] are constants, which depend on material's elasto-plastic properties and indenter tip geometry. These coefficients are not independent and are related by $C = C_p / C_d^2$. The coefficients C_d, C_p, C have been explicitly related to material properties by scaling analysis and finite element simulation of indentation for a homogeneous semispace[19]. To obtain material properties, both P and S are measured at each indentation depth D and from Eq. (1) the coefficients $C_d = D/S$, $C_p = P/S^2$, and $\Lambda = C_p / C_d$ are obtained as functions of indentation depth D.

Prior to thin film testing, the frame compliance of the indentation system was calibrated by evaluating the behavior of the indentation parameters C_d and C_p with depth in a homogeneous fused-silica substrate. For the calibration sample, these parameters should be independent of depth. However, if frame compliance is not properly excluded, these parameters will vary with depth. Thus the correct value of frame compliance is found by evaluating these relations [7].

For all thin film samples listed in Table 1, a series of indentations were performed with maximum indentation depth varying from 100 to 500 nm. The load, indentation depth and contact stiffness were continuously recorded as functions of indentation depth. The corresponding indentation parameters ($C_d = D/S$, $C_p = P/S^2$, and $\Lambda = C_p / C_d$) at each indentation depth were calculated. The effective moduli and hardness of the total film/substrate structures were found using the Oliver-Pharr method[5]. In this method, the effective hardness H_{eff} is computed as

$$H_{eff} = \frac{P}{A}, \tag{2}$$

and the effective modulus E_{eff} as

$$E_{eff} = \frac{\sqrt{\pi} S}{2\beta\sqrt{A}}\,. \tag{3}$$

where A is the projected contact area and β (=1.06) is a constant. The projected contact area A is calculated from the indenter shape function $A=F(D_c)$ extracted from the calibration measurements. The contact depth D_c (Fig. 1a) at indentation depth D is estimated using load P and contact stiffness S:

$$D_c = D - 0.75\frac{P}{S}. \quad (4)$$

In section IV, we discuss two methods for the extraction of the thin film properties from the total effective properties of the structure.

III. RESULTS

A. Substrate characterization

To characterize the film properties, we first performed indentation on the substrate Si(100) wafer. Using the Oliver-Pharr method[5] we obtained a Young's modulus of 179.5 GPa and a hardness of 12.40 GPa, in agreement with data reported elsewhere[10]. The indentation parameters C_d, C_p and C_p/C_d versus indentation depth are shown in Fig. 2. As expected, these parameters are nearly independent of indentation depth. The average value of C_p/C_d is about 0.274.

B. Load-displacement relations

First let us discuss the load-displacement relations. Figures 3(a, b) show the loading-unloading cycles for AG2.2 and AG2.4 samples for maximum indentation depth of 100 nm, 200 nm, 300 nm, 400 nm and 500 nm. At 100nm indentation depth, the loading/unloading cycle is elastic and hysteresis is absent, thus one cannot distinguish the loading and unloading responses in the Figure. For sample AG2.2 (Fig. 3a) at indentation depths of about 200 and 300 nm, "pop-in" events occur (indicated by arrows). These "pop-in" events appear for all "soft" films with smaller thicknesses (AG2.1, AG2.2, and AG1.1). As shown in Figure 3(b) for the thicker film (AG2.4), no "pop-in" events are observed below 500 nm indentation depth. These "pop-in" events may result from film cracking and delamination between the film and substrate.

The ratio between residual displacement D_R after unloading and the maximum indentation depth D_{max} (Fig. 1) is related to the magnitude of plastic deformation underneath the indenter. At smaller maximum indentation depths (100 nm, 200 nm), D_R/D_{max} is very small, which indicates that elastic deformation in the film is dominant. As the indentation depth increases, the ratio D_R/D_{max} increases. Comparing Figure 3a and 3b, we see that the ratio D_R/D_{max} is much higher for thinner films due to significant plastic deformation in the thin soft film induced by the hard substrate constraint. For the thick film (Fig. 3b), the indentation responses are nearly elastic and have only small hysteresis.

Figure 4 compares the load-displacement relations for the samples of Group 1 performed to an indentation depth of 500nm. As expected, films with smaller thickness require higher load for the same penetration and have larger residual displacement due to the substrate effect. The "pop-in" events occur for 450 nm and even 1080 nm thick films.

Figure 5 compares the load-displacement relations for the samples of Group 2. The "pop-in" events occur at lower load for thinner films. Comparing with Figure 4, we see the load is slightly higher at given indentation depth, which indicates these samples are somewhat "stiffer" than the samples of Group 1.

Figure 6 compares the load-displacement relations performed to the 500 nm indentation depth for sample Group 3. Compared to samples of Groups 1 and 2 (Figures 4 and 5), the load is much higher for samples with similar film thicknesses (AG2.3, AG2.2), which indicates these samples are much stiffer. Also no clear "pop-in" events occur for this group within 500 nm indentation depth.

C. C_p and C_p/C_d versus indentation depth

The load-displacement relations provide an intuitive indication of the mechanical properties of the film/substrate system. To further characterize the elasto-plastic properties of the films, we calculated C_p and C_p/C_d from Eq. (1) and plotted them as functions of indentation depth.

The ratio C_p/C_d is a nondimensional parameter related to the ratio between yield stress σ_Y and modulus E [20]. Using scaling analysis and finite element simulations, Wang and Rokhlin [20] have provided explicit scaling functions relating C_p/C_d and σ_Y / E^* ($E^*=E/(1-v^2)$ is the reduced modulus, E is Young's modulus, v is Poisson's ratio and σ_Y is yield stress) for different strain hardening exponents n (Figure 7). When C_p/C_d is close to 0.5, the indentation is dominated by elastic deformation. If C_p/C_d is close to 0.0, significant plastic flow appears underneath the indenter. Thus the experimental parameter C_p/C_d characterizes the levels of contribution of elastic and plastic deformation resulting from a nanoindentation test.

Figures 8, 9 and 10 show C_p/C_d versus indentation depth for the three different groups of samples. To visualize better the initial values at smaller indentation depth, we plotted the indentation depth in logarithmic scale. The C_p/C_d ratio at small depth (flat region where the ratio is independent of depth) may be considered as the "true" film property. However the exact initial value is difficult to define due to noise and surface effects. From Figures 8-10, the approximate "true" C_p/C_d values of all the films is between 0.43 and 0.48, which is very close to the elastic limit 0.5. From Figure 7 (indicated by the shaded area), we find that the yield stress to modulus ratio (σ_Y / E^*)tanθ is between 0.2 and 0.4 (θ is the effective half cone angle=70.3°). The ratio C_p/C_d is a material property, which is a constant for a homogeneous material. For a film/substrate system, C_p/C_d decreases with indentation depth. This is due to the effect of the substrate. One should note that for the Si substrate C_p/C_d is about 0.274 (Section IIIA), i.e. the C_p/C_d ratio for Si is about half of that for the films (0.43-0.48). This allows us to estimate σ_Y / E^* for Si from Figure 7. Due to absence of knowledge of the strain hardening exponent n, one may select n=0.3, a middle value of n, thus σ_Y / E^* for Si is around 0.07/tan(70.3°)=0.025.

The rate of decrease of C_p/C_d is higher for thinner films and the ratio reaches much smaller values than that of the substrate. For example, for sample AG2.2, as shown in Fig. 9, C_p/C_d is less than 0.1 at indentation depth of 490nm, i.e. below that of the substrate (C_p/C_d=0.274). The small C_p/C_d ratio indicates an excess of large nonlinear deformations induced in the film due to the constraint of the hard substrate. These nonlinear residual deformations may be associated with cracking or delamination as indicated in the "pop-in" events in the load-displacement curves for thinner films (Fig. 3a).

Another parameter of interest is C_p =(P/S^2) which is obtained by combining Eqs. (2) and (3) and expressed through the effective hardness H_{eff} and modulus E_{eff} by

$$C_p = \frac{\pi H_{eff}}{4\beta^2 {E_{eff}}^2}, \tag{5}$$

For homogeneous substrates C_p is a constant over indentation depth. The parameter C_p has been used by Saha and Nix [10] for measurements of thin film structures which are nearly elastically homogeneous, such as Al films on glass and W films on sapphire substrate. For an elastically inhomogeneous film/substrate couple the hardness and modulus in Eq. (5) represent the effective properties of the composite film/substrate system, thus C_p will vary with indentation depth characterizing the effect of the substrate during CSM test.

Figure 11(a) shows the parameter C_p in logarithmic scale for the samples of Group 3 (AG3.1, AG3.2, AG3.3). It shows that C_p initially increases and, after reaching a maximum, decreases nearly exponentially as the indentation depth increases. As we'll describe in the next section, the behavior of C_p versus depth is related to the size effect at small indentation depth and a substrate-constraint hardening effect at relatively larger depth. This results in the nonmonotonic behavior of the C_p versus indentation depth shown in Fig. 11(a) and therefore the effective hardness and modulus, as follows from Eq. (5), should have different dependences on depth. At small indentation depth, due to the size effect, both effective modulus and hardness decrease with depth and the growth of C_p versus depth indicates that the decrease rate of the effective modulus squared is larger than that of the effective hardness. At some depth the substrate effect begins to dominate the size effect and effective modulus and hardness increases with depth; this is manifested in the decline of C_p versus depth. Within this region, the increase rate of the effective modulus squared is larger than that of the effective hardness.

Figure 11(b) compares the parameter C_p for the three thicker films (AG1.3, AG2.4, AG3.3) in a linear scale. AG1.3 has the highest peak value of C_p i.e. H_{eff} / E_{eff}^2 ratio. For thicker films, the decrease of the parameter C_p with indentation depth is slower than that for thinner films and as a result sample AG3.3 has the smallest variation of C_p within 500 nm indentation depth..

D. Effective hardness and modulus of the film/substrate systems

In the previous sections we have compared the elasto-plastic properties of the thin film samples using the load-displacement relations and the sbehavior of the parameters C_p/C_d and C_p with depth. In this section the effective hardness and modulus of the film/substrate structures are discussed. As discussed above, the SiCOH film have high C_p/C_d ratio indicating that for small indentation depth the plastic deformation is not significant and "piling-up" around the contact surface is not expected. Thus the Oliver-Pharr method[5] is suitable for modulus and hardness determination. Figures 12(a, b) compare the effective hardness and modulus versus indentation depth normalized to film thickness for samples of Group 1. Figure 12(a) shows that at small indentation depth, the hardness decreases with increase of indentation depth. This decrease results from the indentation size effect[16-18]. This effect has been observed for a soft metal film on a hard substrate and has been studied using strain gradient plasticity theory[16-18]. The hardness reaches a minimum value at a normalized indentation depth between 0.15 and 0.3. Beyond that it increases with indentation depth. Because the film is much softer than the substrate and the indenter tip has not yet reached the substrate, it is expected that there is no plastic deformation in the substrate. Thus this hardness increase with indentation depth is caused by plastic flow constraint in the film resulting in strong gradients of plastic strain in the film between the indenter and substrate. For thicker films, the hardness minimum is smaller and it reaches that minimum value at smaller normalized indentation depth. For thinner films (AG1.1) we observe a sudden drop of hardness at normalized depths of 0.46 and 6.7. These drops correspond to the "pop-in" events shown in Fig. 4 resulting from film cracking and delaminations on the interface.

Figure 12(b) presents the effective moduli versus normalized depth for samples of Group 1. At very small indentation depth, the effective modulus is between 4.5 to 7 GPa. Thinner films have slightly larger values, which is consistent with the slightly larger hardness for thinner films shown in Figure 12(a). As indentation depth increases, the effective modulus increases rapidly and its value for indentation depth equal to the film thickness is five times its initial value. The growth rate with relative indentation depth is almost the same for all four samples in the group. This fast growth rate is expected due to the significant mismatch in modulus between the film and substrate. The "pop-in" events have almost no effect on the modulus measurement.

The effect of the substrate is much stronger on the effective modulus than on the hardness (Fig.12a). This is because the effective modulus is related to the indenter-induced elastic deformation, which has a long range effect and is more strongly affected by the substrate constraint compared to plastic deformation, associated with the hardness (for soft films, the substrate will not be plastically deformed before the indenter tip reaches the substrate).

Figures 13(a, b) show the hardness and modulus versus normalized indentation depth for samples of Group 2. Compared with Groups 1, the samples in Group 2 have slightly higher hardness at given normalized indentation depth. The sudden drop of hardness due to "pop-in" has also been observed at normalized indentation depths above 0.4. Figure 13(b) represents the moduli versus normalized depth for Group 2. At very small indentation depth, the effective modulus is between 6 to 10 GPa.

Figures 14(a, b) depict the hardness and modulus versus normalized indentation depth for samples of Group 3. Figure 14(a) shows the effective hardness. Compared to hardness for samples in Groups 1 and 2, the samples in this Group have the highest hardness. For given normalized indentation depth, thinner films have larger hardness. The sudden drop of hardness shown in Figures 12(a) and 13(a) is not observed in Figure 14(a) because the "pop-in" events are absent in Fig. 5. Figure 14(b) presents the moduli versus normalized depth for Group 3. At very small indentation depth, the effective modulus is between 14 to 18 GPa which is much larger than that of Group 1. Again thinner films have slightly higher moduli. As shown in Figs. 12(b)-14(b) for all samples, when the normalized indentation depth is above 0.2, the effective modulus, which is plotted in logarithmic scale, increases nearly exponentially as indentation depth increases.

IV. DISCUSSION

In the previous sections we presented the experimental results for the SiCOH/Si film/substrate systems. The effective modulus and hardness have been calculated using the Oliver-Pharr method. The properties obtained are the effective properties of the film/substrate system. For soft and thin films, the substrate has significant effect on the effective modulus, as shown in Figures 12-14. Here we will use two methods to determine the intrinsic film properties from the measured effective properties.

A. Film hardness

As shown in Figures 12a, 13a and 14a, the hardness decreases initially due to indentation size effects[16, 17] (it is a near-surface film effect) and then increases due to hardening associated with the constraint of the stiffer substrate. The hardness value at the minimum plateau in the hardness vs. indentation depth curve is taken to be the hardness of the film. This is an approximation

since the minimum position may be affected by the effects of competition of the strain-plasticity gradient and the substrate (see also ref. 10). The hardness values for each sample are given in column three in Table 2. The samples in Group 3 have the smallest hardness. Thinner films have larger hardness values.

B. Film modulus measured using King's method

The modulus of SiCOH is much lower than that of the Si(100) substrate. Therefore the modulus obtained by the Oliver-Pharr method[5] is the effective modulus E_{eff} and will be strongly affected by the stiff substrate. To decouple the substrate effect, we used a relation between the effective and film moduli developed by King[15]. Based on numerical simulation of triangular punches indenting a layered isotropic elastic half-space, they related the effective modulus E_{eff} to film E_f and substrate E_s moduli as a function of projected contact area A and film thickness t

$$\frac{1}{E_{eff}} = \frac{1-\nu_i^2}{E_i} + \frac{1-\nu_f^2}{E_f}(1-e^{-\alpha t/\sqrt{A}}) + \frac{1-\nu_s^2}{E_s}e^{-\alpha t/\sqrt{A}}, \tag{6}$$

where E_i is the modulus and ν_i is the Poisson's ratio of the diamond indenter. α is a parameter which is a function of $\sqrt{A}/t$. By fitting the numerical results provided by King[15] it may be empirically represented as

$$\alpha = 0.2715 + 0.8719\left(\sqrt{A}/t\right)^{1/2} . \tag{7}$$

The projected contact area A is related to contact stiffness S and effective modulus E_{eff} by Eq. 3. One should note that recently Saha and Nix [10] modified King's eq. (6) to account for the Berkovich indenter geometry; however we have found that the original King's eq. (6) is better suited to our thin film systems.

As follows from Eq. (6), the effective modulus of the film/substrate is a weighted summation of the film and substrate moduli. The weights depend on the ratio between the contact radius and the film thickness. The contact area was estimated by the Oliver-Pharr method[5] at each indentation depth D and corresponding load P and contact stiffness S using the indenter shape function and Eq. 4. Substituting the obtained contact area A and stiffness S into Eq. (3) the experimental effective modulus E_{eff} is obtained. Thus the experimental relation between E_{eff} and A was obtained at each given indentation depth D. Using least-square optimization and minimizing the difference between experimental and predicted (from Eq. 6) effective moduli, the film modulus E_f was determined.

Experimental data at very small indentation depth are affected by measuring noise and size effects and at large indentation depth the results are affected by material cracking and interface delamination, thus to obtain the "true" film modulus E_f we have selected for the inversion of Eq. (6) the experimental effective modulus in the range of indentation depths 40 - 250 nm. Figure 15 shows an example for sample AG2.4 of the fitting between the calculated (open squares) and experimental (solid circles) effective modulus. The film moduli determined for all samples are summarized in column five of Table 2. As expected, Group 3 has the largest modulus and Group 1 the smallest. In each group, thinner films have larger modulus. The film modulus determined by this method is smaller than the effective modulus at the initial indentation depth which is shown in column four of Table 2.

B. Finite element simulation and inversion

To further verify the film modulus determination, we have obtained the film modulus by directly comparing the experimental load-displacement relation with finite element (FEM)

indentation simulations. A finite element model with large deformation plasticity similar to those described in Wang & Rokhlin [19] and Knapp et al[21] was used to compute the load-depth relation. In the FEM model, the film and substrate are considered as elastoplastic solids with linear strain-hardening:

$$\sigma = \begin{cases} E\varepsilon, & \varepsilon < \sigma_Y / E \\ \sigma_Y + M_p\varepsilon, & \varepsilon \geq \sigma_Y / E \end{cases}, \tag{8}$$

where E is Young's modulus, σ_Y is yield stress and M_p is plastic strain hardening modulus. The substrate properties are assumed to be known. By comparing the calculated load-depth relation with the experimental one the film properties (E, σ_Y, M_p) are obtained. As an example Figure 16 compares a loading/unloading indentation cycle obtained by the finite element simulations and experiment for sample AG3.2.

The film moduli E_f and the ratio σ_Y/E_f obtained from finite element simulations are given in the sixth and seventh columns of Table 2 respectively. The modulus obtained by the FEM method has reasonable agreement with the modulus obtained using King's model. As discussed in the previous section, using the measured parameter C_p/C_d one obtains from Figure 7 the ratio between yield stress and modulus (σ_Y / E_f) which is between 0.08 and 0.18 for all samples. The FEM results for this ratio scatter around mean value 0.15. Using FEM simulations we also have computed the effective modulus E_{eff} at various indentation depths. The results for sample AG2.4 are shown as solid triangles in Figure 15. This shows that the effective modulus obtained from the unloading curve by the FEM simulations is slightly smaller than that obtained by the CSM measurements.

The modulus and hardness as functions of film thickness are shown in Figures 17 and 18. Dashed lines show the trend. As the film thickness decreases, both modulus and hardness increase. This show that film thickness has significant effect on the extracted mechanical properties measured for thickness below 1 μm. Similar phenomena of the dependence of thin film mechanical properties on thickness have been observed for other thin film systems[10, 18]. The property change may be attributed to either variation of the mechanical properties of the films with thickness or from insufficient deconvolution of the substrate and size effects. Further study is warranted to address this important issue.

Figure 19 compares the difference between the "true" film modulus, E_f, versus the minimum effective modulus, E^{OP}. The minimum of the effective modulus, E^{OP}, is due to the competition between the indentation size (strain gradient plasticity) and substrate constraint effects. In our case this occurred at indentation depth slightly less than 10% of the film thickness, as shown in Fig. 12-14. The difference between E_f and E^{OP} for stiffer films (Group 3) is much smaller than that for soft films (Group 1 and Group 2) at all film thicknesses. The modulus of such films can be evaluated with reasonable accuracy using the indentation at 10% thickness criterion for films thicker than 0.5 micron. For soft films the difference is significant and it decreases, as expected, with increasing film thickness. Defining the modulus of the Group 1 and Group 2 films by the effective modulus at indentation depths of less than 1 micron can give, according to Figure 9, an overestimate up to 35%.

V. CONCLUSIONS

The continuous-stiffness nanoindentation method was used to measure the mechanical properties (effective modulus and hardness) of the film/substrate system for three groups of low-

k to ultralow-k SiCOH films with dielectric constants from 2.4 to 3.0. The parameters C_d, defined as the ratio between indentation depth D and contact stiffness S, and C_p, defined as the ratio between load P and S^2, are obtained as functions of indentation depth. Loading-unloading indentation cycles with different indentation depths have also been obtained. For softer films with a smaller dielectric constant, "pop-in" events were observed in the loading-unloading cycles due to cracks and delaminations formed during indentation. As a result of competition between surface and substrate constraint effects the effective hardness and modulus depend nonmonotonically on indentation depth. At small indentation depth, both hardness and modulus first decrease with indentation depth due to size and strain gradient plasticity effects, then reach a minimum and increase with further increment of indentation depth due to the substrate constraint effect. At relative large indentation depth, modulus increases nearly exponentially with indentation depth.

The "true" film properties were determined using both an empirical formulation for the effective modulus and direct inversion based on a finite element model. Both methods are in reasonable agreement. The average hardness and modulus for Group 1 films with dielectric constants=2.4 are around 0.79 GPa and 4.2 GPa respectively, for Group 2 films with dielectric constants=2.7 are around 1.15 GPa and 5.6 GPa, for Group 3 films with dielectric constants=3.0 are around 2.3 GPa and 13.7 GPa. For each group with the same dielectric constant thinner films usually have higher modulus and hardness.

While for stiffer films of Group 3 the modulus measured at an indentation depth of 10% of film thickness is close to the "true" value, for films thicker than 0.5 micron, the measured value can give an overestimate up to 35% for softer films of Groups 1 and 2, under the same conditions.

References

1. A. Grill, "Plasma enhanced chemical vapor deposited SiCOH dielectrics: from low-k to extreme low-k interconnect materials," J. Appl. Phys. **93**, 1785 (2003).
2. A. Grill and D. A. Neumayer, "Structure of low dielectric constant to extreme low dielectric constant SiCOH films: Fourier transform infrared spectroscopy characterization," J. Appl. Phys. **94**, 1 (2003).
3. A. Grill and V. Patel, "Ultralow-k dielectrics prepared by plasma-enhanced chemical vapor deposition," Appl. Phys. Lett. **79**, 803 (2001). 3a . D. Edelstein, C. Davis, L. Clevenger, M. Yoon, A. Cowley, T. Nogami*, H. Rathore, B. Agarwala, S. Arai**, A. Carbone, K. Chanda, S. Cohen, W. Cote, M. Cullinan, T. Dalton, S. Das, P. Davis, J. Demarest, D. Dunn, C. Dziobkowski, R. Filippi, J. Fitzsimmons, P. Flaitz, S. Gates, J. Gill, A. Grill, D. Hawken, K. Ida*, D. Klaus, N. Klymko, M. Lane, S. Lane, J. Lee, W. Landers, W-K. Li, Y-H. Lin, E. Liniger, X-H. Liu, A. Madan, S. Malhotra, J. Martin#, S. Molis, C. Muzzy, D. Nguyen, S. Nguyen, M. Ono**, C. Parks, D. Questad, D. Restaino, A. Sakamoto*, T. Shaw, Y. Shimooka**, A. Simon, E. Simonyi, S. Tempest, T. Van Kleeck, S. Vogt, Y-Y. Wang, W. Wille, J. Wright, C-C. Yang, and T. Ivers, Reliability, Yield, and Performance of a 90 nm SOI/Cu/SiCOH Technology, *Proceedings of the IEEE 2004 Intern. Interconnect Technol. Conference*, IEEE, Piscataway, NJ (IEEE Catalog No. 04TH8729) (2004) p 214.

[4] A. Grill, V. Patel, K. P. Rodbell, E. Huang, M. R. Baklanov, K. P. Mogilnikov, M. Toney, and H. C. Kim, "Porosity in plasma enhanced chemical vapor deposited SiCOH dielectrics: a comparative study," J. Appl. Phys. **94**, 3427 (2003).

[5] W. C. Oliver and G. M. Pharr, "An improved technique for determining hardness and elastic modulus using load and displacement sensing indentation experiments," J. Mater. Res. **7**, 1564 (1992).

[6] Fischer-Cripps, A. C. *Nanoindentation*, Mechanical Engineering Series, Springer-Verlag 2002.

[7] W. C. Oliver and G. M. Pharr, "Measurement of hardness and elastic modulus by instrumented indentation: advances in understanding and refinements to methodology," J. Mater. Res. **19**, 3(2004).

[8] J. Menčik, D. Munz, E. Quandt, E. R. Weppelmann, and M. V Swain, "Determination of elastic modulus of thin layers using nanoindentation," J. Mater. Res. **12**, 2475 (1997).

[9] W. D. Nix, "Elastic and plastic properties of thin films on substrates: nanoindentation techniques," Mater. Sci. Eng. **A234**, 37 (1997).

[10] R. Saha and W. D. Nix, "Effects of the substrate on the determination of thin film mechanical properties by nanoindentation," Acta Mater. **50**, 23 (2002).

[11] L. Shen, K. Zeng, Y. Wang, B. Narayanan, and R. Kumar, "Determination of the hardness and elastic modulus of low-k thin films and their barrier layer for microelectronic applications," Microelectronic engineering **70**, 115 (2003).

[12] A. A. Volinsky, J. B. Vella, and W. W. Gerberich, "Fracture toughness, adhesion and mechanical properties of low-K dielectric thin films measured by nanoindentation," Thin Solid Films **429**, 201 (2003).

[13] T. Y. Tsui, C. A. Ross, G. M. Pharr, "A method for making substrate-independent hardness measurements of soft metallic films on hard substrates by nanoindentation," J. Mater. Res. **18**, 1383 (2003).

[14] T. Y. Tsui, G. M. Pharr, "Substrate effects on nanoindentation mechanical property measurement of soft films on hard substrates," J. Mater. Res. 14, 292 (1998).

[15] R. B. King, "Elastic analysis of some punch problems for a layered medium," Int. J. Solids Struct. **23**, 1657 (1987).

[16] W. D. Nix and H. Gao, "Indentation size effects in crystalline materials: a law for strain gradient plasticity," J. Mech. Phys. Solids **46** , 411(1998).

[17] R. Saha, Z. Y. Xue, Y. Huang, and W. D. Nix, "Indentation of a soft metal film on a hard substrate: strain gradient hardening effects," J. Mech. Phys. Solids **49**, 1997 (2001).

[18] Z. H. Xu and D. Rowcliffe, "Deriving mechanical properties of soft coatings using nanoindentation: an application of mechanism-based strain gradient plasticity," Surf. and Coatings Tech. **157**, 231 (2002).

[19] L. Wang and S. I. Rokhlin, "Universal scaling functions for continuous stiffness nanoindentation with sharp indenters," Int. J. Solids Struct., submitted (2004).

[20] L. Wang and S. I. Rokhlin, "Inverse scaling functions in nanoindentation with sharp indenters: determination of material properties," J. Mater. Res., submitted (2004).

[21] J. A. Knapp, D. M. Follstaedt, S. M. Myers, J. C. Barbour, and T. A. Friedmann, "Finite element modeling of nanoindentation," J. Appl. Phys. **85**, 1460 (1999).

Figure Captions

FIG. 1. (a) Schematic of the indentation on a film/substrate system, material sinking-in, $a_i > a$. (b) Illustration of a typical loading and unloading response and notation. In CSM, a small sinusoidal force is added to the static load and the corresponding displacement response is recorded.
FIG. 2. Experimental indentation parameters C_d, C_p for Si (100) substrate.
FIG. 3. Load vs. indentation depth for (a) sample AG2.2 (b) sample AG2.4 for different maximum indentation depth. Arrows indicate the "pop-in" events.
FIG. 4. Load vs. indentation depth for samples of Group 1. Arrows indicate the "pop-in" events.
FIG. 5. Load vs. indentation depth for samples of Group 2. Arrows indicate the "pop-in" events.
FIG. 6. Load vs. indentation depth for samples of Group 3.
FIG. 7. Solid lines are simulated relation between C_d / C_p and σ_Y / E^* for different strain hardening exponents n. The experimental values C_d / C_p for Si (100) are indicated by dotted lines. The experimental values C_d / C_p for the SiCOH films are indicated by the shaded region.
FIG. 8. C_p/C_d indentation depth for samples of Group 1.
FIG. 9. C_p/C_d vs. indentation depth for samples of Group 2.
FIG. 10. C_p/C_d vs. indentation depth for samples of Group 3.
FIG. 11. (a) C_p vs. indentation depth for samples of Group 1. (b) C_p vs. indentation depth for thick film samples AG1.3 (1950 nm), AG2.4 (1340 nm), AG3.3 (4000 nm).
FIG. 12. (a) Effective hardness and (b) modulus of the SiCOH/Si structure for samples of Group 1 (AG1.1 (450 nm), AG1.2 (1080 nm), AG1.3 (1950 nm)). Arrows indicate the "pop-in" events.
FIG. 13. (a) Effective hardness and (b) modulus of the SiCOH/Si structure for samples of Group 2 (AG2.1 (370 nm),AG2.2 (410 nm), AG2.3 (900 nm), AG2.4 (1340 nm)). Arrows indicate the "pop-in" events.
FIG.14. (a) Effective hardness and (b) modulus of the SiCOH/Si structure for samples of Group 3 (AG3.1 (500 nm), AG3.2 (1000 nm), AG3.3 (4000 nm)).
FIG. 15. Comparison between experimental results, finite element simulations and King's model for sample 2.4.
FIG. 16. Experiment and finite element simulation of loading-unloading indentation cycle for sample 3.2.
FIG. 17. The effect of film thickness on the film modulus. Dashed lines indicate trends.
FIG. 18. The effect of film thickness on the film hardness. Dashed lines indicate trends.

	Specimen	Dielectric constant	Thickness (nm)
Group 1	AG1.1	2.4	450
	AG1.2	2.4	1080
	AG1.3	2.4	1950
Group 2	AG2.1	2.7	370
	AG2.2	2.7	410
	AG2.3	2.7	900
	AG2.4	2.7	1340
Group 3	AG3.1	3.0	500
	AG3.2	3.0	1000
	AG3.3	3.0	4000

Table 1. Sample description.

1	2	3	4	5	6	7
	Specimen	Hardness (GPa)	Modulus (E^{OP}) (GPa)	Modulus (E_f) (GPa)	Modulus (FEM) (GPa)	σ_Y / E_f^* (FEM) (GPa)
Group 1	AG1.1	0.92	6.7	5.0	4.9	0.14
	AG1.2	0.76	5.2	3.9	4.0	0.22
	AG1.3	0.70	4.7	3.7	3.6	0.21
Group 2	AG2.1	1.1	7.5	5.8	5.0	0.26
	AG2.2	1.5	10.5	6.8	7.0	0.14
	AG2.3	1.0	6.6	4.9	4.8	0.21
	AG2.4	1.0	6.0	4.9	4.7	0.21
Group 3	AG3.1	2.7	18.4	17.1	17.0	0.09
	AG3.2	2.3	14.8	12.8	15.0	0.10
	AG3.3	2.0	13.9	11.3	13.0	0.11

Table 2. Measured hardness and modulus and calculated film parameters..

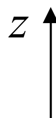

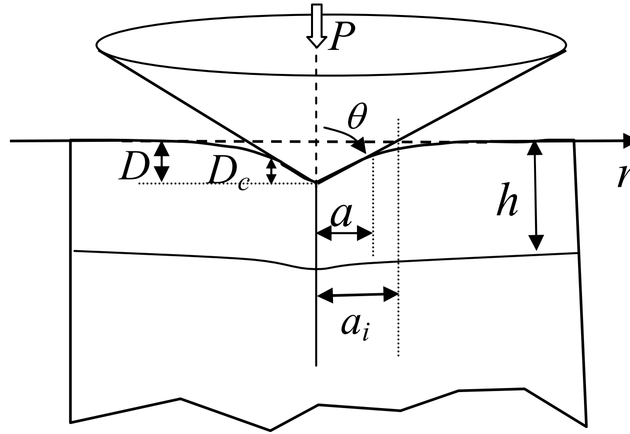

(a)

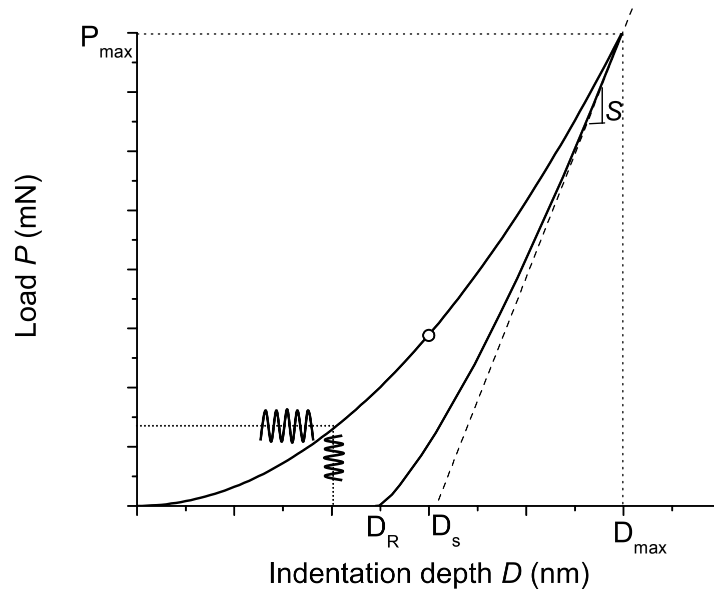

(b)

FIG. 1. (a) Schematic of the indentation on a film/substrate system, $a_i > a$ *indicates that* material is sinking-in. (b) Illustration of a typical loading and unloading response and used notations. In CSM, a small sinusoidal force is added to the static load and the corresponding displacement response is recorded.

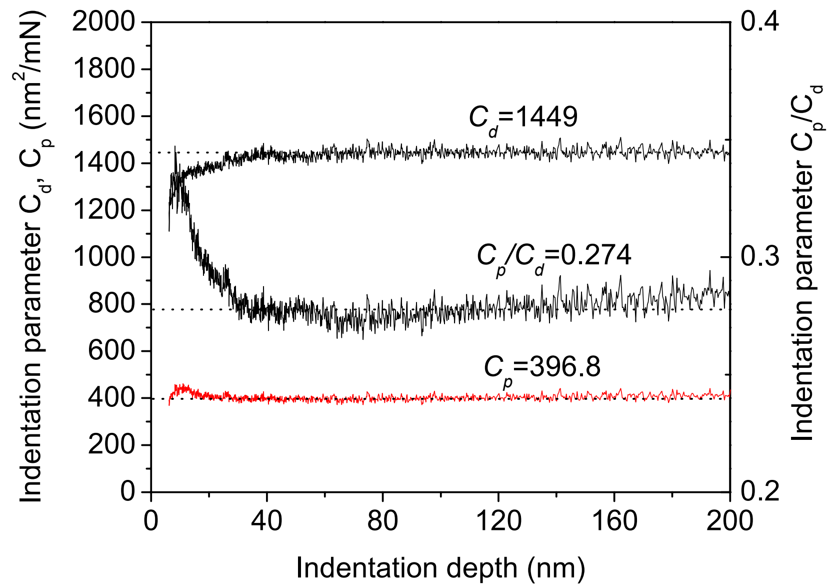

FIG. 2. Experimental indentation parameters C_d, C_p for Si (100) substrate.

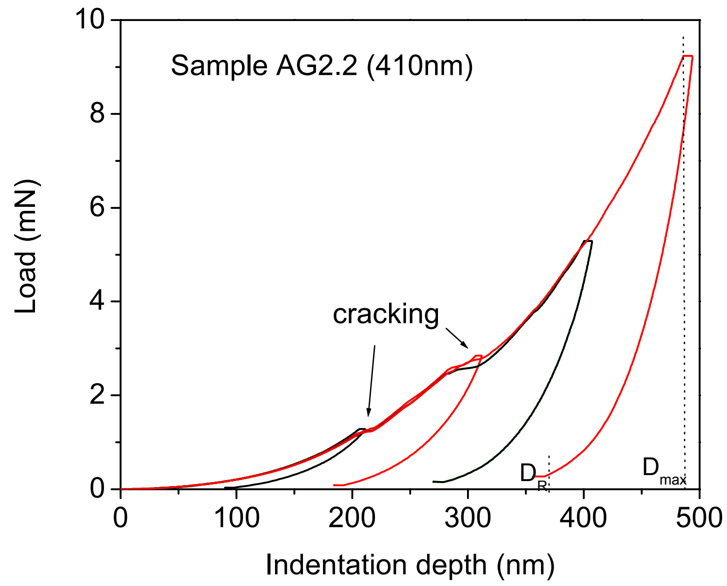

(a)

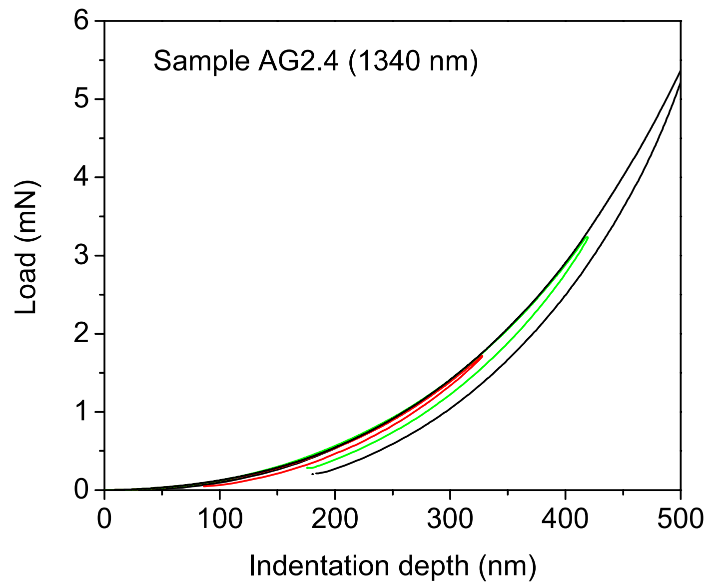

(b)

FIG. 3. Load vs. indentation depth for different maximum indentation depths. (a) sample AG2.2 (b) sample AG2.4. Arrows indicate the "pop-in" events.

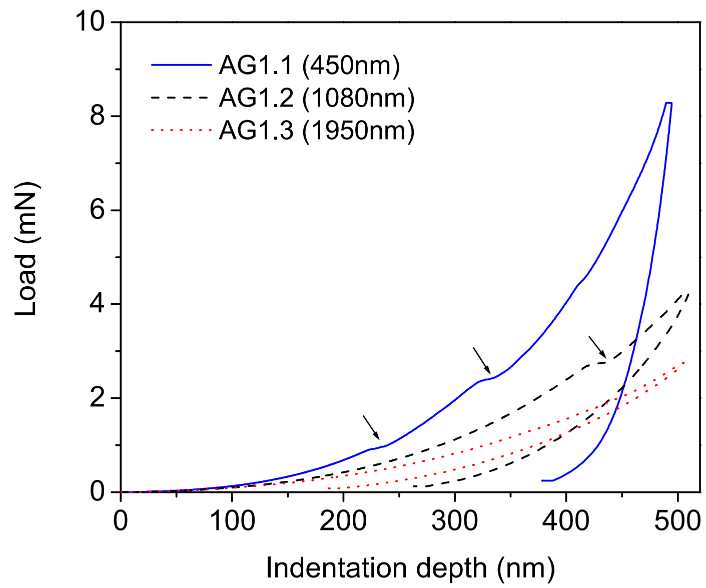

FIG. 4. Load vs. indentation depth for samples of Group 1. Arrows indicate the “pop-in” events.

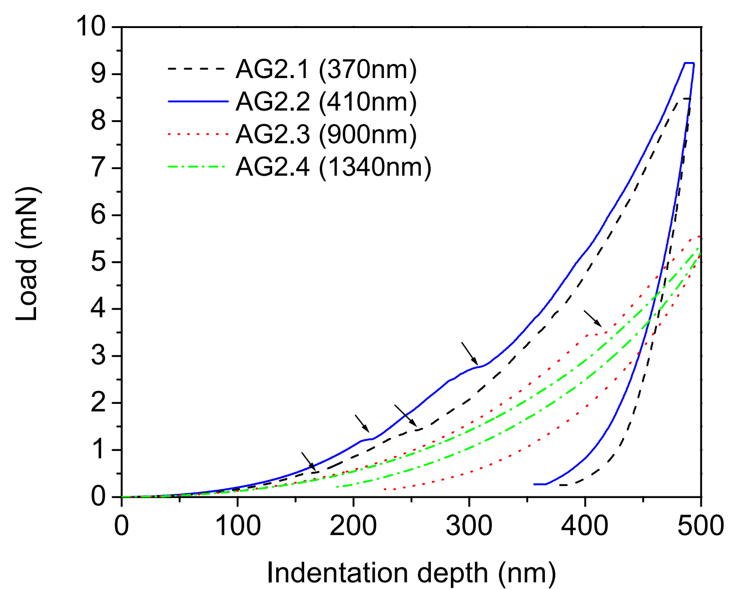

FIG. 5. Load vs. indentation depth for samples of Group 2. Arrows indicate the “pop-in” events.

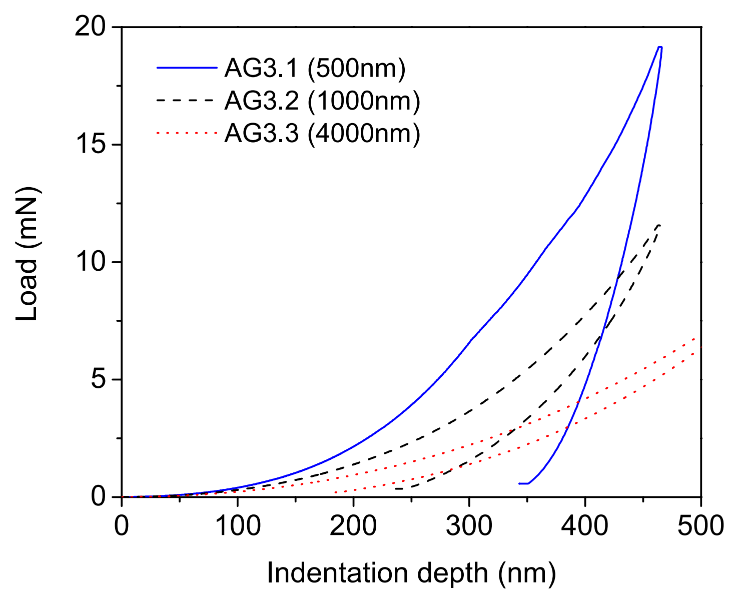

FIG. 6. Load vs. indentation depth for samples of Group 3.

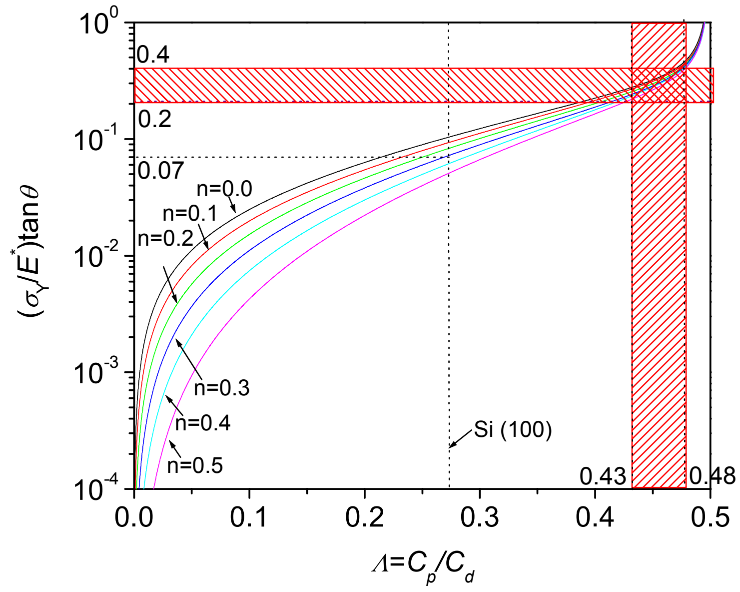

FIG. 7. Simulated relations between C_d / C_p and σ_Y/E^* for different strain hardening exponents *n* (solid lines). The experimental values C_d / C_p for Si (100) are indicated by dotted lines. The experimental values C_d / C_p for the SiCOH films are indicated by the shaded region.

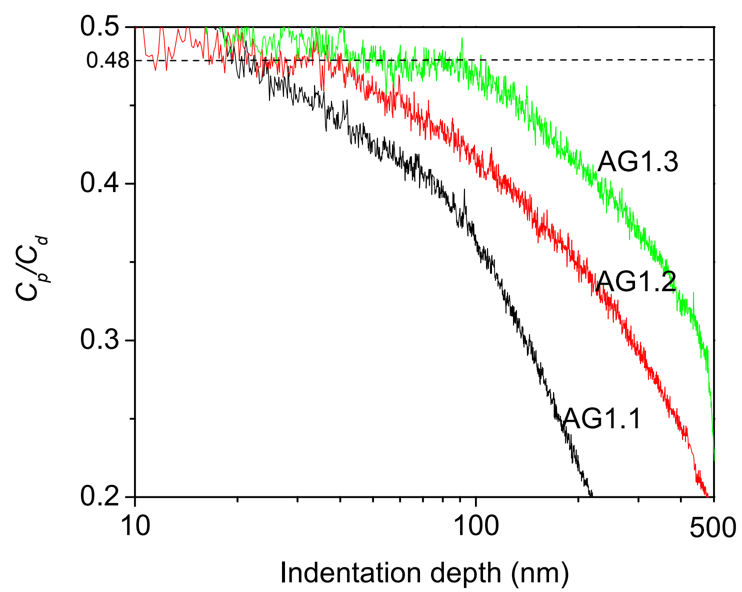

FIG. 8. C_p/C_d vs. indentation depth for samples of Group 1.

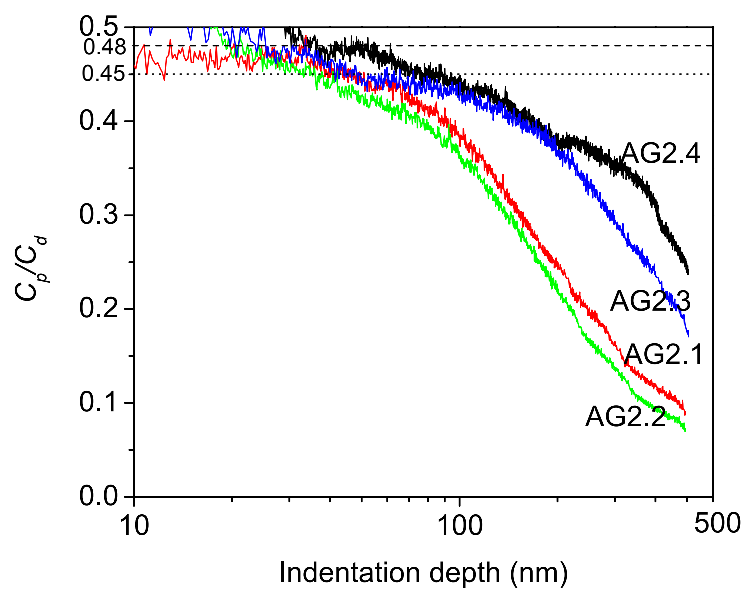

FIG. 9. C_p/C_d vs. indentation depth for samples of Group 2.

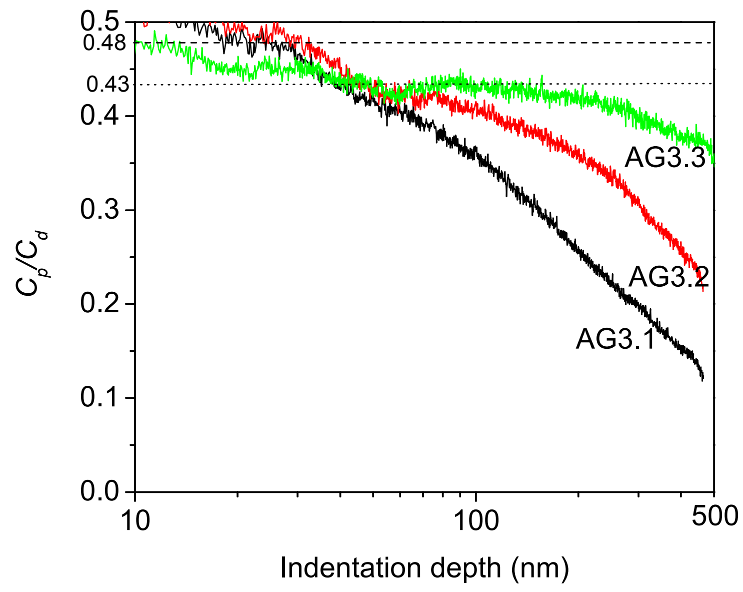

FIG. 10. C_p/C_d vs. indentation depth for samples of Group 3.

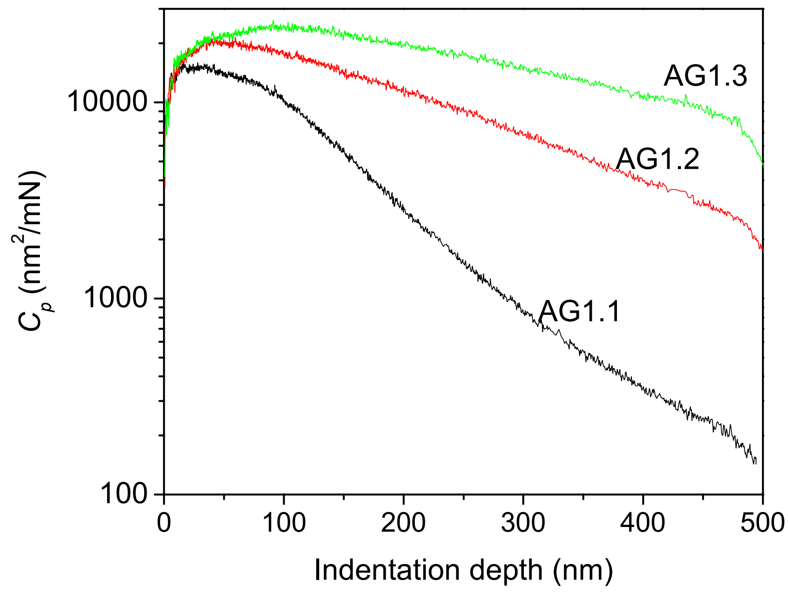

(a)

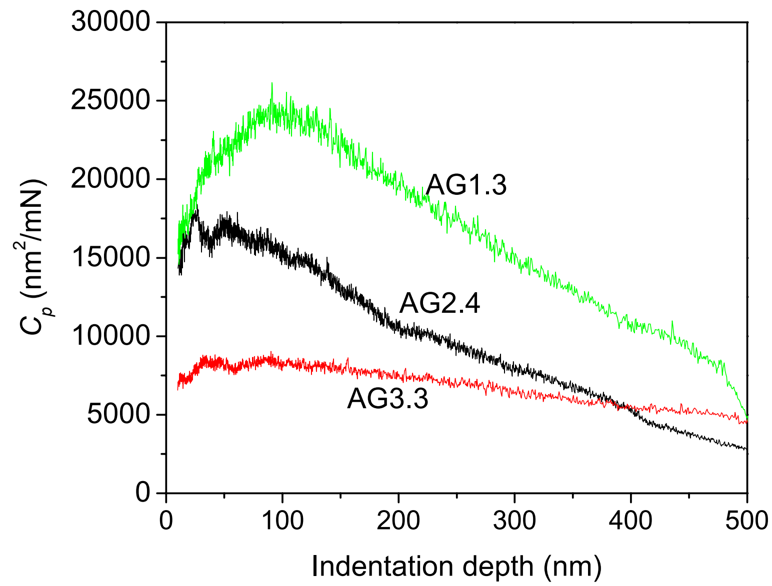

(b)

FIG. 11. C_p vs. indentation depth: (a) for samples of Group 1. (b) for thick film samples AG1.3 (1950 nm), AG2.4 (1340 nm), AG3.3 (4000 nm).

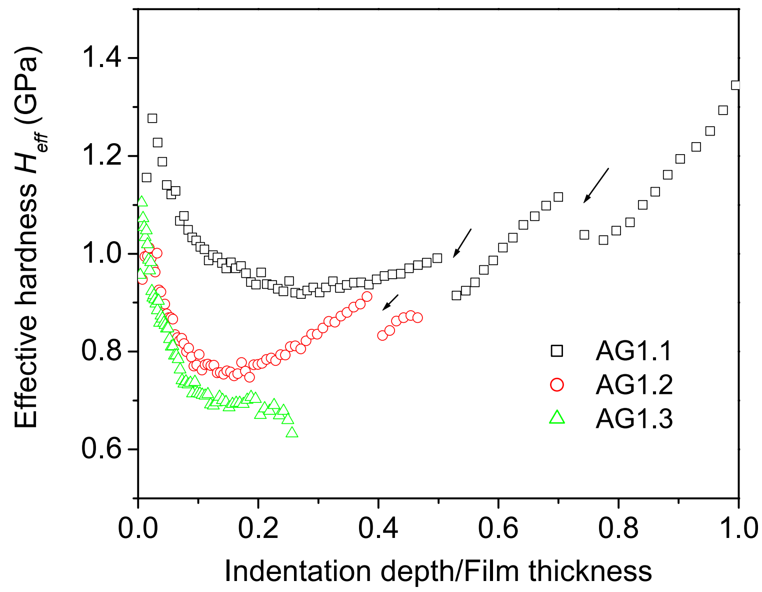

(a)

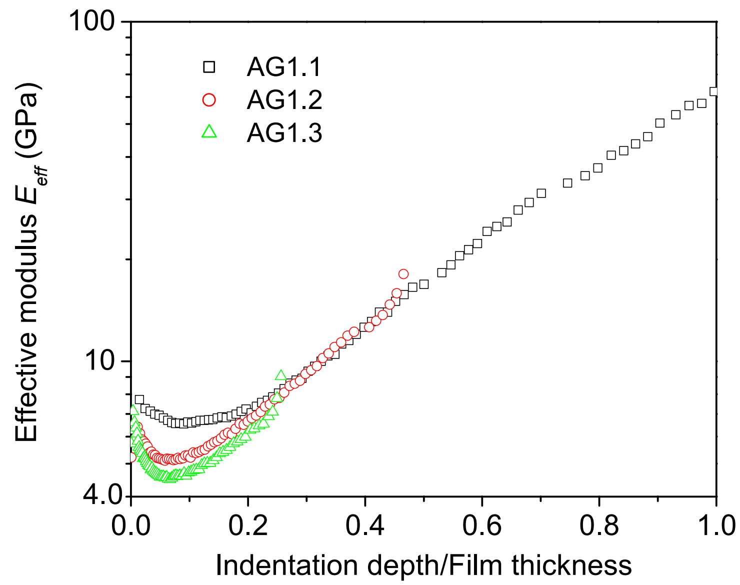

(b)

FIG. 12. Effective hardness (a) and modulus (b) of the SiCOH/Si structure for samples of Group 1 (AG1.1 - 450 nm), AG1.2 -1080 nm, AG1.3 - 1950 nm). Arrows indicate the “pop-in” events.

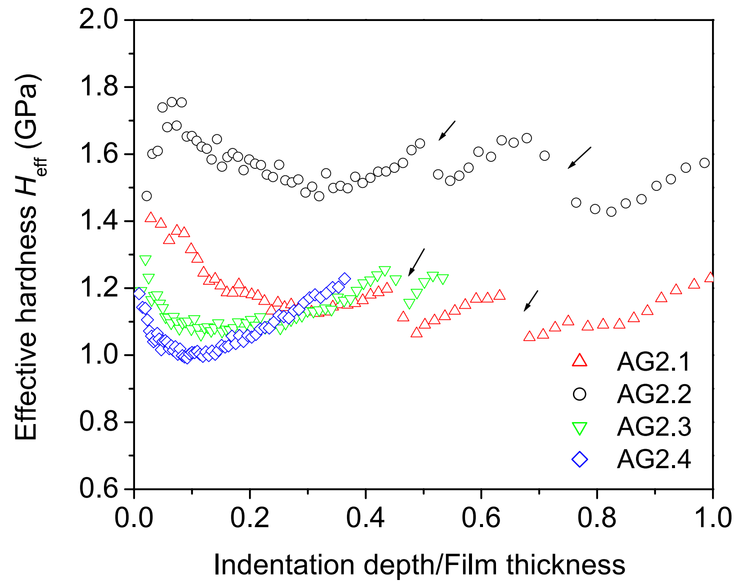

(a)

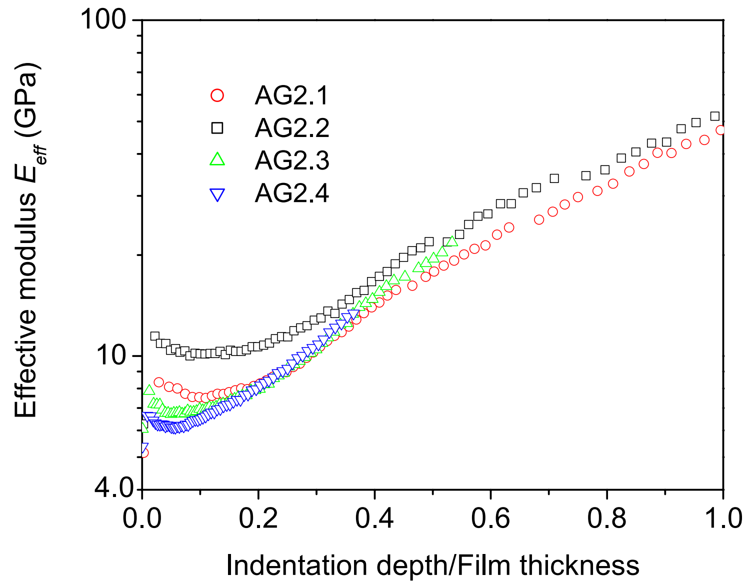

(b)

FIG. 13. (a) Effective hardness (a) and (b) modulus(b) of the SiCOH/Si structure for samples of Group 2 (AG2.1 - (370 nm), AG2.2 (- 410 nm), AG2.3 (- 900 nm), AG2.4 (-1340 nm)). Arrows indicate the "pop-in" events.

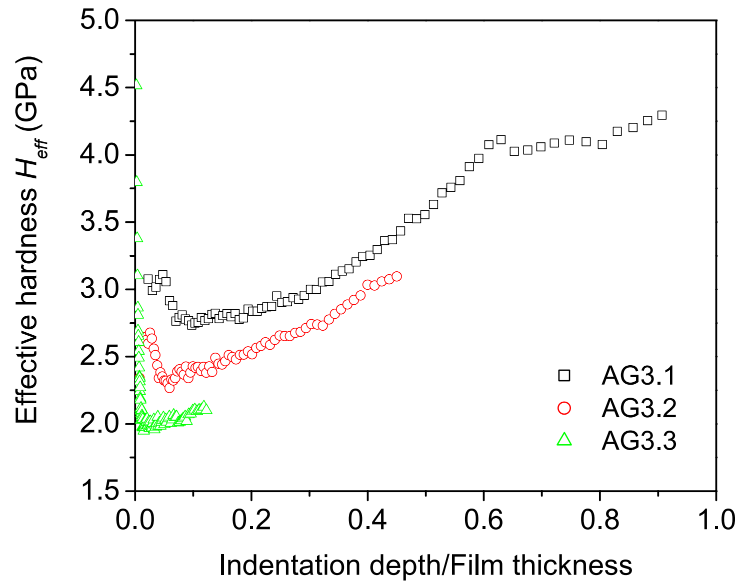

(a)

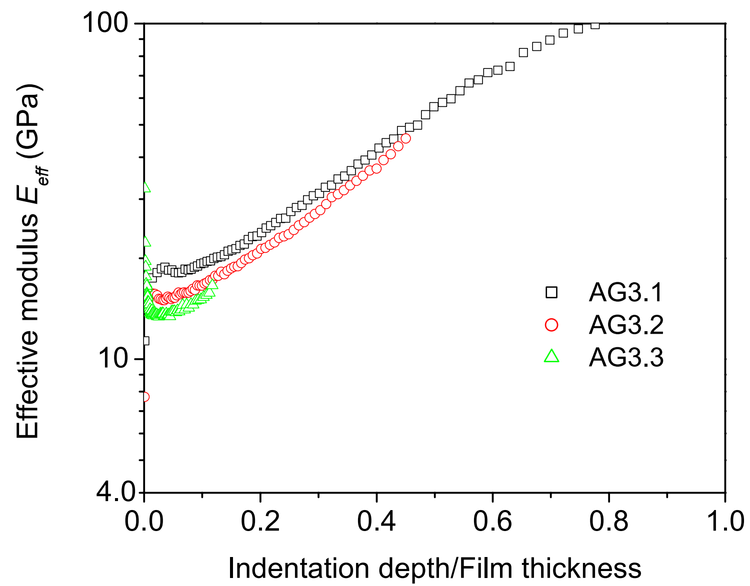

FIG.14. (a) Effective hardness (a) and (b) modulus(b) of the SiCOH/Si structure for samples of Group 3 (AG3.1 - (500 nm), AG3.2 -(1000 nm), AG3.3 - (4000 nm)).

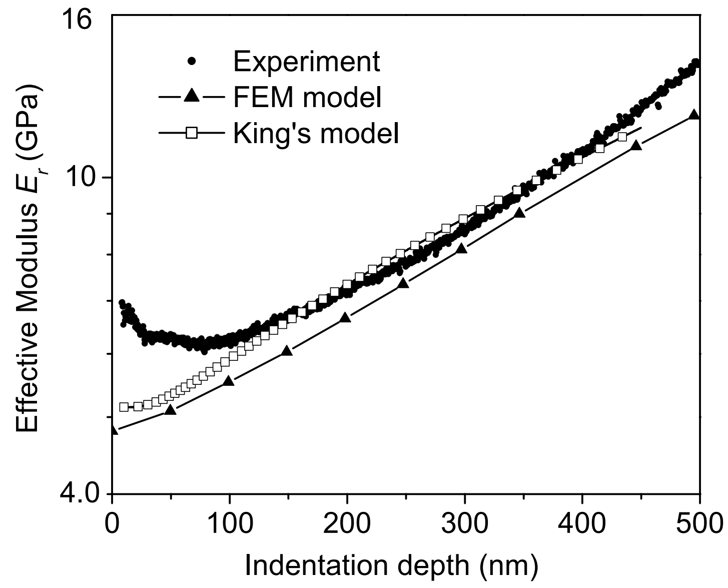

FIG. 15. Comparison between experimental results, finite element simulations and King’s model for sample AG2.4.

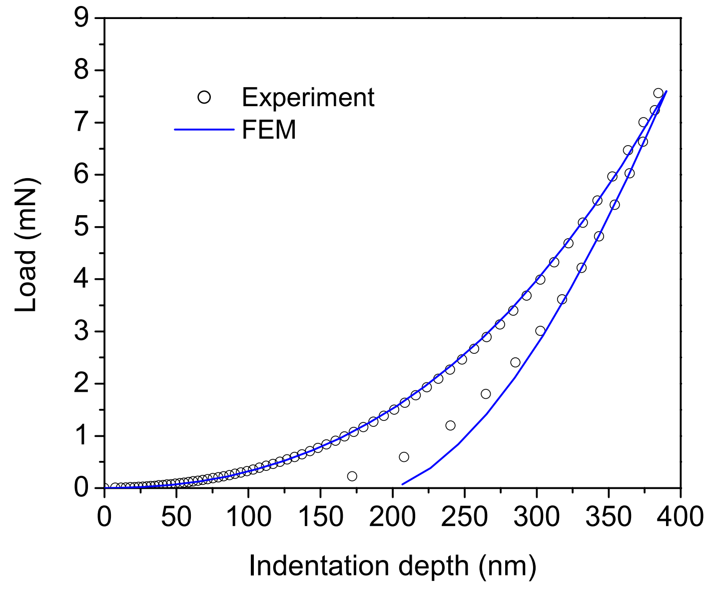

FIG. 16. Experiment and finite element simulation of loading-unloading indentation cycle for sample AG3.2.

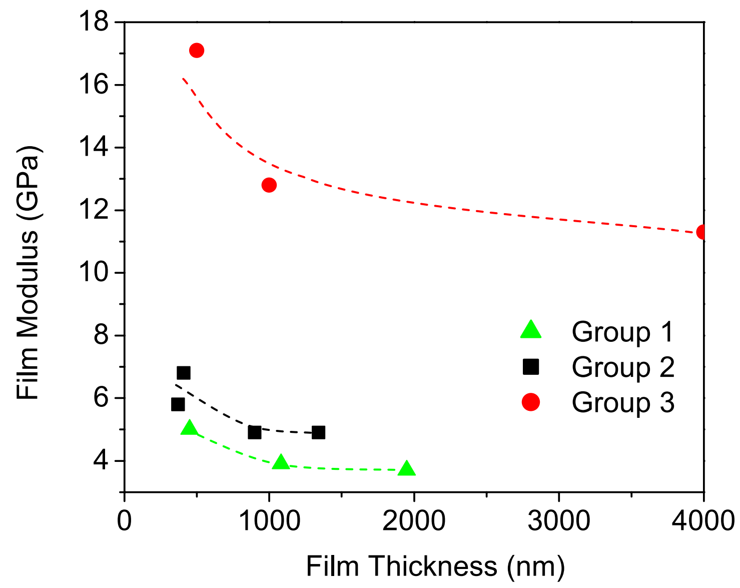

FIG. 17. The effect of film thickness on the film modulus. Dashed lines indicate trends.

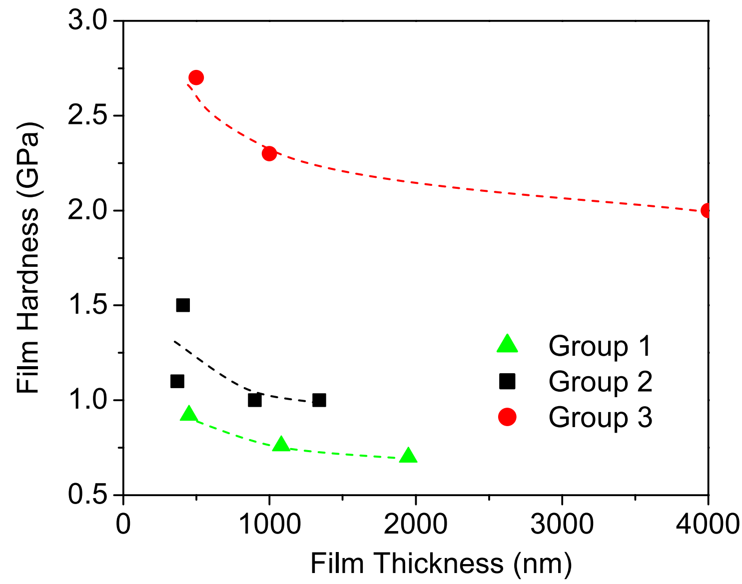

FIG. 18. The effect of film thickness on the film hardness. Dashed lines indicate trends.

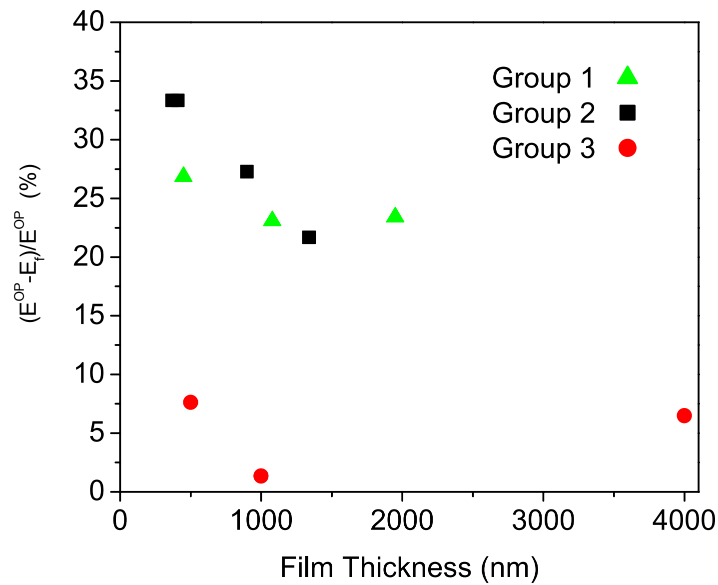

FIG. 19. Difference between the "true" film modulus E_f and the effective modulus E^{OP} measured at indentation depth of modulus minimum (Figs.12-14), at about 10% of the film thickness.